

THE POROUS PLATES OF CONIFORM CHLORIDE CELLS IN MAYFLY LARVAE: HIGH-RESOLUTION ANALYSIS AND DEMONSTRATION OF SOLUTE PATHWAYS

H. KOMNICK AND W. STOCKEM

*Institut für Cytologie und Mikromorphologie der Universität Bonn,
5300 Bonn 1, Gartenstr. 61a, BRD, W. Germany*

SUMMARY

The porous plates of coniform chloride cells in mayfly larvae were studied by electron microscopy using carbon replicas, whole-mount cuticles and thin sections. The cuticular skeleton of the porous plates is a local differentiation of the epicuticle forming a structure of extremely high organization. It is composed of cylindrical rods, which measure 20 nm in diameter, and are oriented perpendicular to the cuticular surface. They form an overlapping hexagonal pattern and are interconnected by double rows of transverse bars which are arranged in a complicated but regular fashion. This spongy skeleton defines a continuous space system which may be characterized as composed of triangular pores, the sides of which measure 20 nm. The pores are arranged in a hexagonal pattern, and interconnected via slit-like communications. The porous plates are covered with a porous lamina which possesses 2.5-nm-wide pores in hexagonal arrangement.

Results obtained from negative staining, infiltration with colloidal lanthanum hydroxide and histochemical precipitation of sodium indicate that the porous system provides pathways for solutes across the cuticle.

The 3-dimensional architecture of the porous plates is reconstructed in a model that also includes morphogenetic aspects.

INTRODUCTION

The coniform chloride cells of mayfly larvae have been shown to absorb chloride from dilute external solutions and to be involved in osmoregulation (Komnick, Rhees & Abel, 1972). The conical apex of these cells lies inside a funnel-shaped recess of the cuticle and is covered by a porous plate, which is approximately 0.1 μm thick and constitutes a specialized cuticular boundary between the chloride cell and the outside medium (Wichard & Komnick, 1971; Komnick & Abel, 1971; Wichard, Komnick & Abel, 1972). Since the apices of the chloride cells are involved in ion trapping and accumulation, the porous plates must permit permeation of ions and, therefore, are regarded as specialized sites of high cuticular permeability. Accordingly, the porous plates provide an important link in the function of the chloride cells, in particular with respect to the initial step of ion adsorption. Therefore, the fine architecture of the plates was investigated with the use of different preparative techniques in order to elucidate the transcuticular pathway of salt.

MATERIALS AND METHODS

The porous plates of the coniform chloride cells were studied by electron microscopy in 3 mayfly species of the family Baetidae, namely *Baetis rhodani*, *Callibaetis* cf. *coloradensis*, and *Cloeon dipterum*.

Whole-mount cuticles. Shed cuticles were collected after moult and washed in distilled water for several days. The sternites or tergites of the abdominal segments were isolated with fine tweezers and either positively or negatively stained. For positive staining the cuticles were immersed in 1% aqueous phosphotungstic acid at pH 2.2 or 1% uranyl acetate for 30 min, washed in 3 changes of distilled water and mounted on Formvar-coated grids. For negative staining the cuticles were first mounted on grids and subsequently covered for 30–60 s with a drop of 1% phosphotungstic acid containing 0.1% sucrose and 0.01% egg albumen at pH 5.0 (Reimer, 1967).

Carbon replicas. The larvae were fixed with 2% osmium tetroxide in 0.1 M cacodylate buffer at pH 7.2 and dehydrated in graded ethanols. The abdominal cuticles were carefully peeled off the dehydrated specimens and digested under control by a treatment with Packard Sample Solubilizer Soluene TM 100 for 0, 1, 2, 5, 10, 20 and up to 80 h. After washing out the Soluene in several changes of absolute ethanol, the cuticles were rehydrated and mounted on gelatine-coated aluminium platelets. The air-dried cuticles were transferred to an Edwards vacuum evaporator and shadowed with carbon during rotation at 40° tilt. After dissolving the gelatine supporting layer, the shadowed cuticles were placed in 40% chromic acid for 3 days, until they were completely dissolved. The remaining replicas were subsequently washed in several changes of 10% ethanol and distilled water and mounted on grids.

Thin sections. For fine-structural investigation the tracheal gills were fixed with 2% osmium tetroxide in 0.1 M cacodylate buffer at pH 7.2, stained *en bloc* with 1% aqueous phosphotungstic acid, dehydrated in graded ethanols and embedded in styrene-methacrylate (Kushida, 1961) or Araldite (Glauert & Glauert, 1958). Thin sections were cut perpendicular or parallel to the gill surface with the LKB ultratome and stained with lead citrate in some cases (Venable & Coggeshall, 1965). For penetration studies fixation was performed in 1% osmium tetroxide containing 1.5% colloidal lanthanum hydroxide (Revel & Karnovsky, 1967). For histochemical precipitation of sodium, the tracheal gills were fixed in a mixture of 2% osmium tetroxide and 2% potassium pyroantimonate at pH 8.0 (Komnick, 1962).

All preparations were studied with a Philips EM 300 electron microscope. Pictures were taken with the plate camera at magnifications up to 160 000 times.

OBSERVATIONS

In carbon replicas the porous plates of the coniform chloride cells are readily identifiable by their nearly uniform size and particularly by their circular rim, which in the majority of the plates possesses a knob-like protrusion (Fig. 1). The pores themselves, however, are normally invisible in replicas made from untreated cuticles because they are covered with a thin additional layer. This layer is completely dissolved by prolonged treatment with Soluene, so that the pores become visible in replicas made from treated cuticles (Fig. 1). After a short treatment with Soluene a honeycomb pattern of fine lines appears (Fig. 2), which could not be demonstrated by any of the additional preparation techniques used. Therefore, the structural components underlying this pattern remain unclarified. With progressively extended treatment small depressions of irregular sizes and outlines appear at the corners of the hexagons (Fig. 3). These indentations subsequently increase in size and attain a more regular outline with concomitant disappearance of the honeycomb pattern (Fig. 4). Finally, a hexagonal pattern of triangular pores is revealed (Fig. 5). The triangles are nearly equilateral with sides measuring 20 nm. Each triangle is surrounded by 3 others in

such a way that each side of the central triangle lies parallel to one side of an adjacent triangle at a distance of 15 nm. Within the hexagonal arrangement 1 corner of each of the 6 triangles is pointing to the centre. The facing corners of each pair of opposite triangles lie 60 nm apart.

The interpretation that the triangles seen in carbon replicas actually represent the pores is confirmed by the results obtained on differently stained whole-mount cuticles and thin sections (Figs. 6–9), although the dimensions are slightly different in the different preparations.

In whole-mount cuticles positively stained with phosphotungstic acid (Fig. 6) the pores appear as light, electron-transparent triangles with rounded corners due to the decrease in resolution which is caused by the relatively thick layer of the porous plate. They are arranged in hexagonal rosettes which overlap in such a way that each pair of rosettes has 2 pores in common. The centre of each rosette is occupied by a black, electron-absorbing structure which represents a cuticular rod in vertical projection. The rods measure 20 nm in diameter; they are regularly placed at equidistant positions with centre-to-centre distances of 40 nm and interspaces of 20 nm. This arrangement results in a triangular pattern, which in turn forms an overlapping hexagonal pattern. Each rod is connected with 6 surrounding rods by a spoke-like structure. Negatively stained preparations (Fig. 7), which yield micrographs of higher resolution, and the analysis of tangential and cross-sections of the plates (Figs. 8–10), clearly reveal that this structure is composed of 6 double rows of transverse bars, which measure 20 nm in length and 4–5 nm in diameter. After lanthanum infiltration and when viewed in vertical projection many bars exhibit a central black dot. It is uncertain whether this is an artifact or indicative of penetration of lanthanum into a hollow core. In tangential sections (Figs. 8, 9) the double rows are figured as pairs of parallel transverse bars, the individual bars of the pairs lying 4–5 nm apart and adjacent pairs always forming angles of 60° due to the hexagonal arrangement of the rods. In appropriate cross-sections of the porous plates (Fig. 10) the bars figured as circles in vertical projection are clearly seen to be piled up in straight double rows at interspaces of approximately 4.0 nm. Although there are slight irregularities, the individual rows are shifted relative to each other in such a way that the bars of one row are facing the interspaces between the bars of the second row (Fig. 10). This indicates that the individual bars of each pair are located at different levels. Furthermore, the interspaces between the bars provide slit-like transverse communications between the pores. Consequently, the entire pore system is a continuous space interlarded with cuticular rods and bars which form an interconnected structure of extremely high and regular organization. The various patterns of the rods and transverse bars obtained in cross-sections of the porous plates (Figs. 10, 12–14) can be explained by different thicknesses and planes of the sections (Fig. 29).

Negatively stained whole-mount cuticles (Fig. 7) show a reverse contrast when compared with positively stained ones (Fig. 6). This demonstrates that phosphotungstic acid under the conditions of negative staining is able to penetrate into the pores and the interspaces between the transverse bars, but not into the bars and rods themselves. The same holds true for colloidal lanthanum as seen in tangential and

cross-sections of the porous plate (Figs. 9, 10). The picture obtained from tangential sections of the porous plates of specimens fixed in the colloidal lanthanum/osmium mixture (Fig. 9) is the same as that of the porous plates in negatively stained cuticles (Fig. 7) but reversed in contrast compared to the pictures of tangential sections of porous plates positively stained with phosphotungstic acid during dehydration (Fig. 8). Hence, the pores can be unequivocally identified by comparison of positively and negatively stained whole-mount cuticles and thin sections. This identification differs from the interpretation given previously (Komnick & Abel, 1971).

After fixation with both the osmium/pyroantimonate solution for histochemical precipitation of sodium and the osmium/silver lactate solution for precipitation of chloride, dense precipitates have been found in rows within the porous plates of the chloride cells (cf. Wichard & Komnick, 1971; Komnick *et al.* 1972). Figs. 23 and 24 clearly demonstrate that the antimonate precipitates are confined to the pores. These results obtained from negative staining, lanthanum infiltration and antimonate precipitation reveal that the pores of the porous plates in ephemerid chloride cells provide pathways for solutes across the cuticle.

The porous plates are roughly diskoidal in shape. Their thickness is of the order of magnitude of $0.1 \mu\text{m}$. At the external surface they are covered by an additional layer which is approximately $7.5\text{--}15.0 \text{ nm}$ in thickness. At high magnifications this layer shows regular cross-striations (Fig. 18). After infiltration with lanthanum the contrast of the striations is converse (Fig. 19) indicating that lanthanum is also able to penetrate into this layer. In tangential sections the lanthanum is confined to small dots (Figs. 21, 22), reflecting the presence of small pores. Therefore this layer is termed the porous lamina. The pores measure approximately 2.5 nm in diameter, lie about 2.5 nm apart, and are arranged into triangular patterns, which are grouped into overlapping hexagonal patterns (Fig. 21). In *Callibaetis*, whose porous plates possess an external layer with $0.1\text{--}0.25 \mu\text{m}$ -wide perforations (Fig. 11) (cf. Komnick & Abel, 1971), the porous lamina is discontinuous and is limited to the perforations (Figs. 20, 21).

In lanthanum preparations a thin, light layer is seen overlying the porous lamina (Figs. 19, 20). At places tiny striations which measure $0.5\text{--}1.0 \text{ nm}$ across appear to be present (Fig. 19). However, the question whether these striations also represent pores cannot be definitely answered since these dimensions are at the limit of resolution which can be obtained with thin sections. The striations could likewise be an artifact, which, for example, is caused by the granulate lanthanum staining. If these striations were real the pores of this layer would be of the order of magnitude of a molecular sieve.

The outermost layer of the porous plates is composed of a loose, flocculent or filamentous material (Fig. 18) which stains with lanthanum (Figs. 19, 20). This layer also coats the normal cuticle (Fig. 11) where it represents the cement layer.

According to these observations, the entire porous plate of coniform chloride cells is composed of at least 4 layers. Since the porous plates represent local specializations of the cuticle, the question arises whether there are any correlations between the layers of the porous plates and those of the normal cuticle. According to the terminology of Locke (1964) the normal cuticle of the tracheal gills of the mayfly larvae studied

consists of the procuticle and epicuticle, the latter being composed of (1) dense layer, (2) cuticulin layer, (3) wax layer, and (4) cement layer. The lateral wall of the funnel-shaped recess of the cuticle containing the central cell apex of the chloride cell complexes is apparently formed by the dense layer, since it is similar in contrast and fine structure and continuous with the dense layer of the normal cuticle. The dense layer is also continuous with the porous plate (Figs. 11, 17), although the fine structure of the porous plate is different. Contrary to a previous interpretation (Komnick & Abel, 1971), the entire porous plate is now regarded as homologous with the epicuticle. This is obvious from structural irregularities, which are occasionally found in porous plates of *Baetis*. (1) In one case an incomplete porous plate was observed in which only one-half is differentiated in the typical fashion of porous plates, while the second half consists of a normal epicuticle instead (Fig. 17). (2) The regular pattern of the rods is occasionally disturbed by cuticular material of irregular shape and size (Figs. 15, 16), which fine structurally and in contrast corresponds to the rods on the one hand and to the normal dense layer on the other. It further corresponds to the material of the perforated layer in *Callibaetis* (Fig. 11), which is continuous with the normal dense layer (cf. Komnick & Abel, 1971). Consequently, the rods of the porous plates are probably made up of dense-layer material. It is hard to decide from the morphological observations whether the electron-dense cortex of the rods (Fig. 8) and the transverse bars radiating from this cortex differ in nature from the core of the rods or merely reflect a superficial condensation of the same material constituting the core. The irregularities shown in Fig. 16 seem to suggest that the cortex of the rods and the transverse bars are equivalent to the cuticulin layer, which directly lines the dense layer and exceeds its electron density (Fig. 11). However, the latter interpretation may conflict with the morphogenetic aspects discussed later on page 670, in particular when the morphogenetic role attributed to the cuticulin layer (Locke, 1967) is taken into consideration.

The coordination of the porous lamina also remains unclarified. In contrast it is different from both cuticulin and wax layer and does not show a clear continuity with either. Since at the time of formation the cuticulin layer normally seems to have 2.5–3 nm-wide pores (Locke, 1967), it may be that the porous laminae, including the thin overlying sheath, represent specialized sites of the cuticulin layer which retain the pores.

DISCUSSION

The porous plates of the coniform chloride cells in mayfly larvae consist of at least 2 porous layers which differ in their pore size and structure. The internal layer is a spongy structure of rods and transverse bars, whose meshes can be regarded as pores in the sense of transcuticular pathways. According to this point of view, the internal layer possesses 2 types of pores in the transcuticular direction: triangular pores, the sides of which measure 20 nm, and slit-like pores between the double rows of transverse bars, which measure approximately 5.0×20.0 nm. Of the same size are the slit-like cross communications whereby the total porous space is interconnected. The

external porous lamina apparently has circular pores measuring 2.5 nm in diameter. In *Callibaetis* an additional porous layer is present, which mainly consists of dense-layer material and shows rounded or polygonal perforations 0.1–0.25 μm in width (see also Komnick & Abel, 1971). All these pores are too wide to play any role in the selection of solutes to be absorbed by the chloride cells. If they do not contain some material which is able to select electrolytes, their primary function would be to increase cuticular permeability locally and provide access for the ions to the transporting cells.

In order to understand the 3-dimensional architecture of the porous plates more precisely, attempts were made to reconstruct the arrangements of rods and transverse bars in a model. The first attempts were unsuccessful and were performed by drilling holes along plastic rods in which the transverse bars were inserted according to the structural observations made on cross- and tangential sections. Finally, morphogenetic aspects were also taken into consideration which led to a relatively easy reconstruction of a model (Fig. 25). As seen in cross-sections, each rod has 6 pairs of transverse bars shared with 6 adjacent rods (Fig. 9). The individual rods of any pair are located at different levels (Fig. 10). This implies that there is a repeating structural cycle of 6 transverse bars along the rods. Assuming that the transverse bars pointing in the same direction are deposited at the same time, they are located at the same level. Since this, however, holds true for only one of the paired bars, the second is deposited after a half turn. Consequently, 2 opposing bars are always deposited after 60° turns. This consideration leads to the building unit shown in Fig. 28. Its asymmetrical structure can be explained by a 60° rotation, or considering a chain of these units, by counter-current rotary movements in adjacent rods (Fig. 28). These units can be composed into chains which can be arranged in parallel in a layer, in such a way that the individual chains are alternately shifted by half the centre-to-centre distance of the rods (Fig. 28). The model shown in Fig. 25 was built by piling up such layers, in that the consecutive layers were progressively rotated at 60°. The model fulfils the structural details seen in the electron micrographs (compare Fig. 26 with Figs. 7–9 and 21; and Fig. 27 with Fig. 10), as well as the theory of cuticular morphogenesis that includes rotation movements during thickness growth (Locke, 1967). Therefore this reconstruction may lead towards the understanding not only of the structure but also of the morphogenesis of the highly organized porous plates.

We are grateful for the technical assistance of Miss I. Baas, Mr P. Batta and Mrs I. Stüer.

REFERENCES

- GLAUERT, A. M. & GLAUERT, R. H. (1958). Araldite as an embedding medium for electron microscopy. *J. biophys. biochem. Cytol.* **4**, 191–194.
- KOMNICK, H. (1962). Elektronenmikroskopische Lokalisation von Na⁺ und Cl⁻ in Zellen und Geweben. *Protoplasma* **55**, 414–418.
- KOMNICK, H. & ABEL, J. H., JR. (1971). Location and fine structure of the chloride cells and their porous plates in *Callibaetis* spec. (Ephemeroptera, Baetidae). *Cytobiologie* **4**, 467–479.
- KOMNICK, H., RHEES, R. W. & ABEL, J. H., JR. (1972). The function of ephemerid chloride cells. Histochemical, autoradiographic and physiological studies with radioactive chloride on *Callibaetis*. *Cytobiologie* **5**, 65–82.

- KUSHIDA, H. (1961). A styrene-methacrylate resin embedding method for ultrathin sectioning. *J. Electron Microsc.* **10**, 16-19.
- LOCKE, M. (1964). The structure and formation of the integument of insects. In *The Physiology of Insecta*, vol. 3 (ed. M. Rockstein), pp. 379-470. New York and London: Academic Press.
- LOCKE, M. (1967). The development of patterns in the integument of insects. *Adv. Morphogen.* **6**, 33-88.
- REIMER, L. (1967). *Elektronenmikroskopische Untersuchungs- und Präparationsmethoden*, 2. erw. Aufl. Berlin, Heidelberg and New York: Springer-Verlag.
- REVEL, J. P. & KARNOVSKY, M. J. (1967). Hexagonal array of subunits in intercellular junctions of the mouse heart and liver. *J. Cell Biol.* **33**, C7.
- VENABLE, J. H. & COGGESHALL, R. (1965). A simplified lead citrate stain for use in electron microscopy. *J. Cell Biol.* **25**, 407-408.
- WICHARD, W. & KOMNICK, H. (1971). Electron microscopical and histochemical evidence of chloride cells in tracheal gills of mayfly larvae. *Cytobiologie* **3**, 215-228.
- WICHARD, W., KOMNICK, H. & ABEL, J. H. JR. (1972). Typology of ephemerid chloride cells. *Z. Zellforsch. mikrosk. Anat.* **132**, 533-551.

(Received 4 September 1972)

Fig. 1. Carbon replica of a porous plate in *Cloeon* after prolonged Soluene treatment. *k*, cuticular knob; *s*, surface spines of the cuticle. Notice the margin of dissolved material originally masking the pores. $\times 20000$.

Figs. 2-5. Higher magnifications of carbon replicas made from porous plates after progressively extended Soluene treatment. The sequence of the figures corresponds to increasing periods of treatment. $\times 150000$.

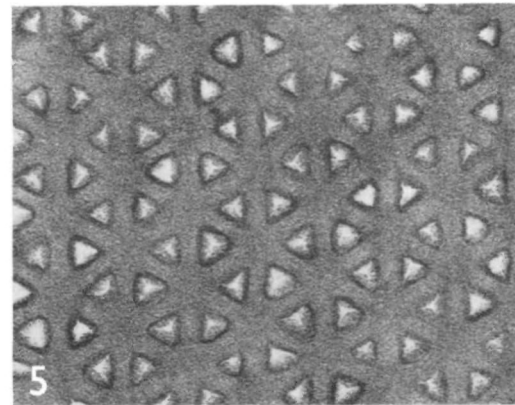
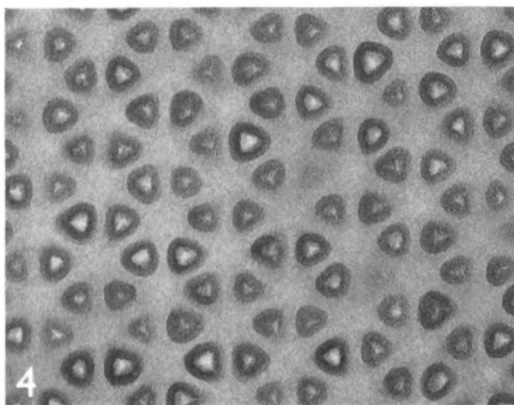
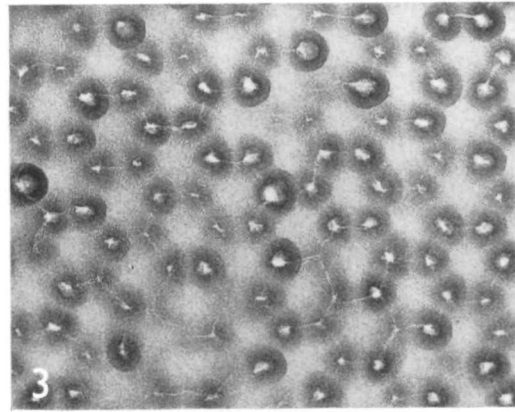
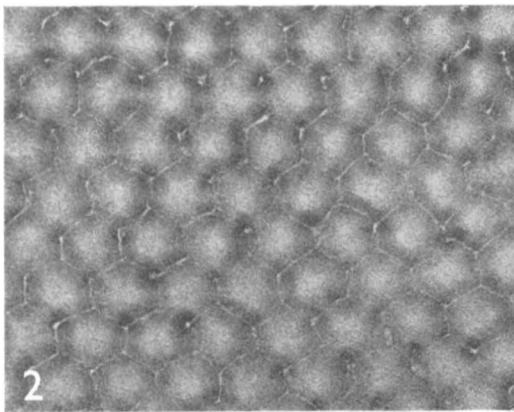


Fig. 6. Transmission electron micrograph of a porous plate in a positively stained whole-mount cuticle of *Cloeon*. $\times 400\,000$.

Fig. 7. The same as Fig. 6, but negatively stained. $\times 400\,000$.

Fig. 8. Tangential section of a porous plate of *Baetis* stained *en bloc* during dehydration. $\times 400\,000$.

Fig. 9. As Fig. 8, but of *Callibaetis*, and infiltrated with colloidal lanthanum during fixation. $\times 400\,000$.

Fig. 10. Cross-section of a porous plate of *Baetis* infiltrated with colloidal lanthanum, showing double rows of the transverse bars in vertical projection. $\times 500\,000$.

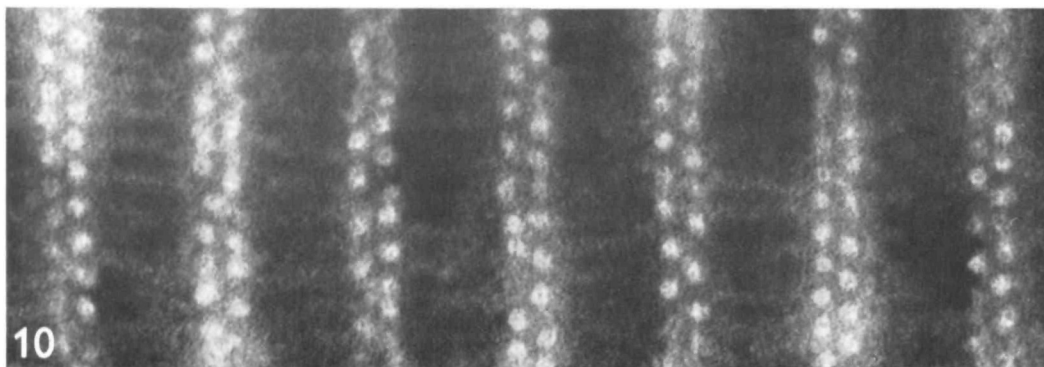
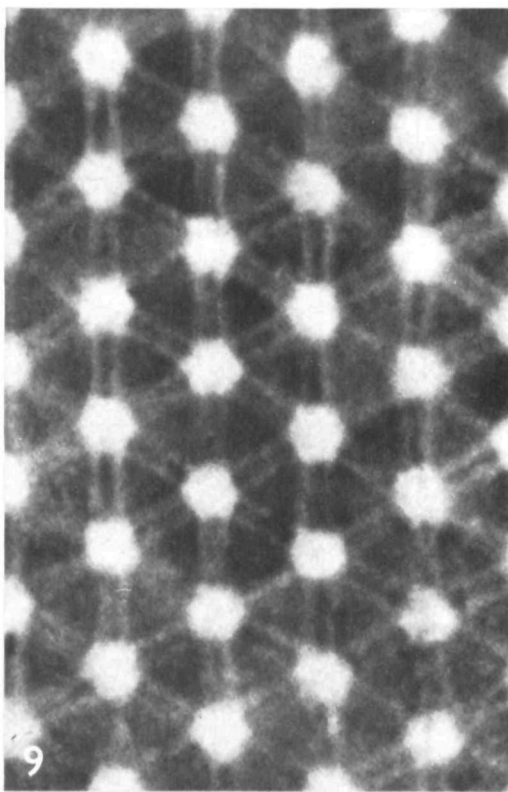
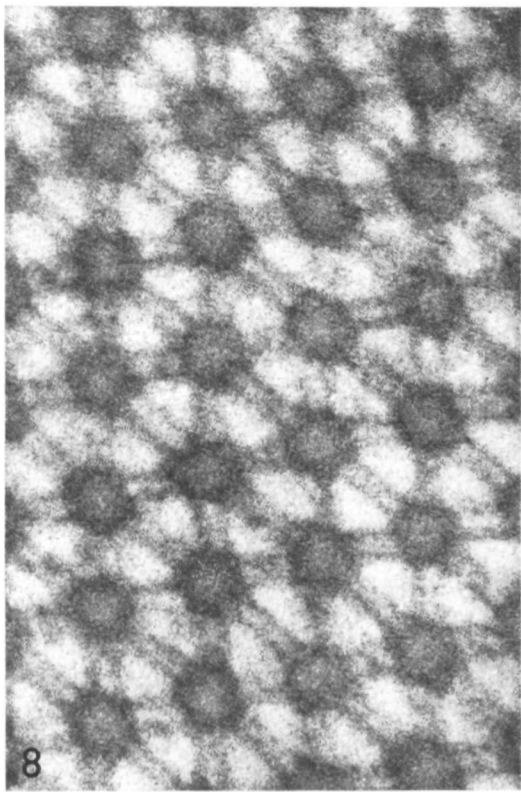
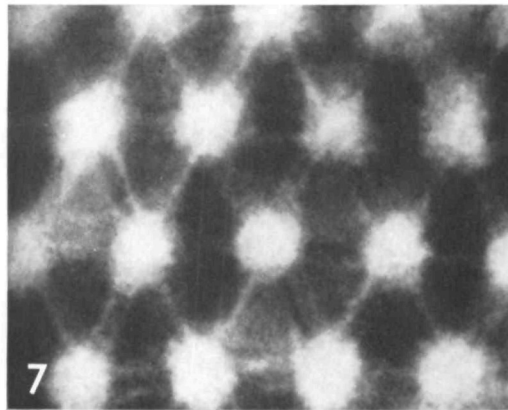
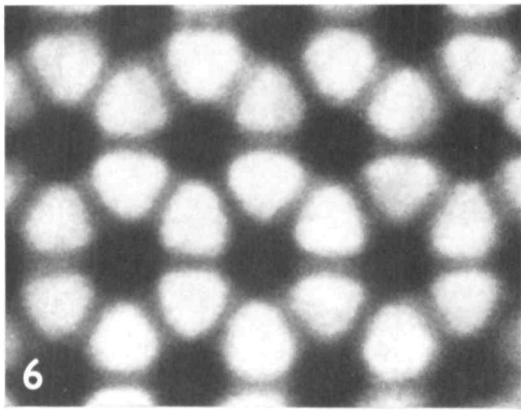


Fig. 11. Peripheral part of a porous plate of *Callibaetis* in cross-section. Notice the dense layer, cuticulin layer, wax layer, and cement layer in the perforated layer and the adjacent normal cuticle. The arrow points to the porous lamina with faintly visible striations which covers the porous plate inside the large perforations. $\times 75\,000$.

Figs. 12–14. Cross-sections of the porous plates of *Baetis* showing different arrangements of rods and transverse bars as a consequence of different thicknesses and planes of the sections relative to architecture of the porous plate (for explanation compare Fig. 29). $\times 300\,000$.

Figs. 15, 16. Structural irregularities of porous plates in *Baetis*. Fig. 15, cross-section; Fig. 16, tangential section. $\times 200\,000$.

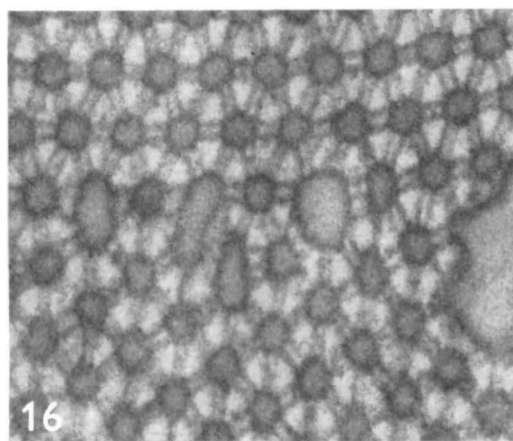
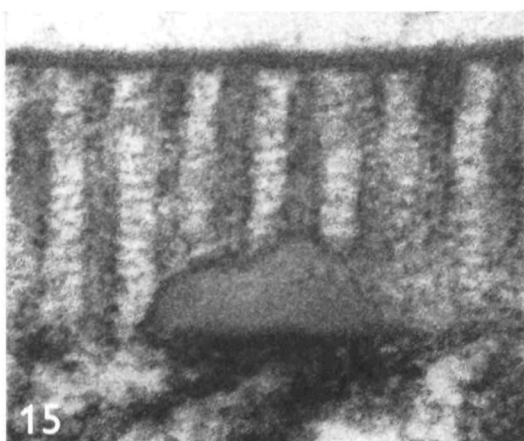
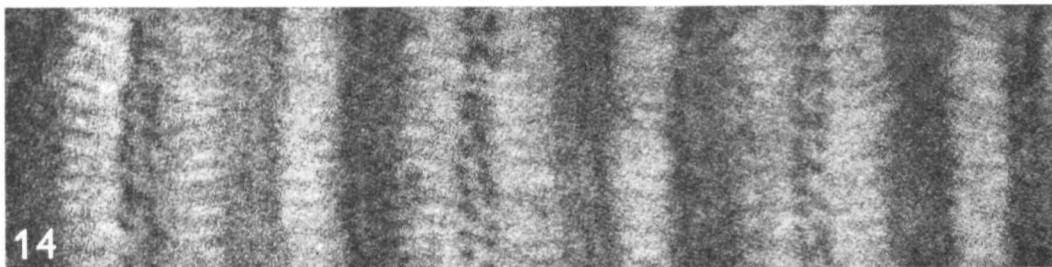
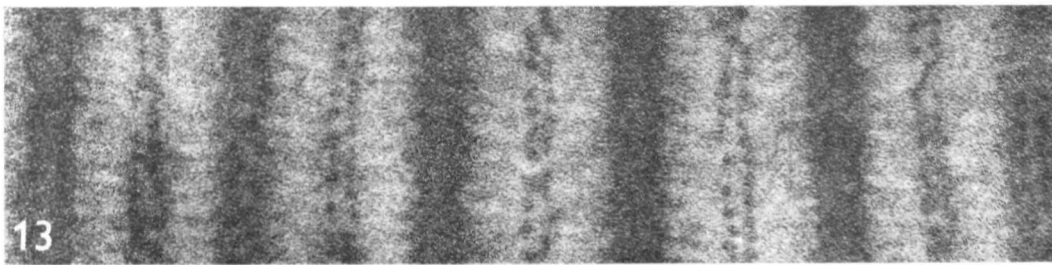
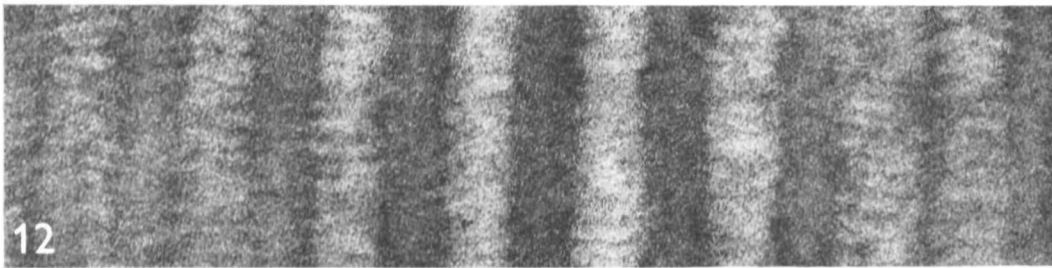
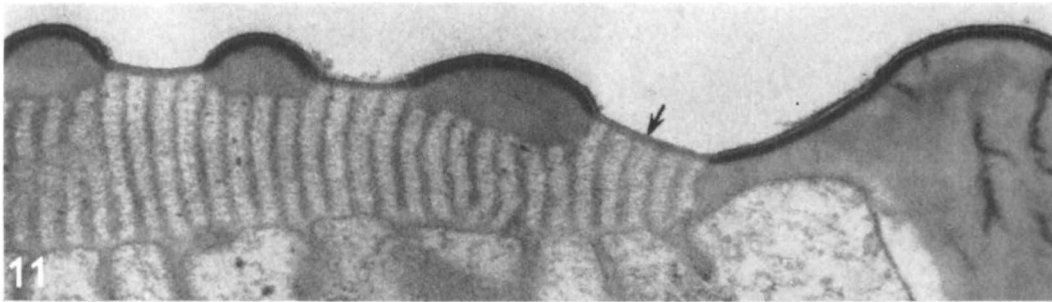


Fig. 17. Cross-section of an incomplete porous plate of *Baetis*. $\times 28000$.

Fig. 18. Cross-section of a porous plate of *Baetis* stained *en bloc* during dehydration and showing the porous lamina and external flocculent coat. $\times 400000$.

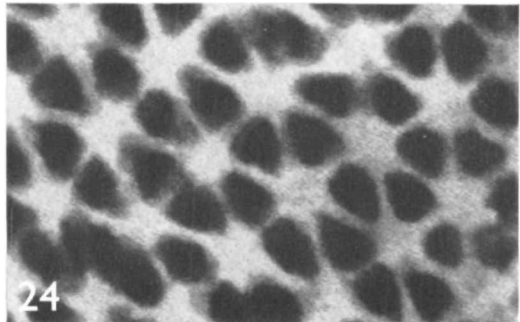
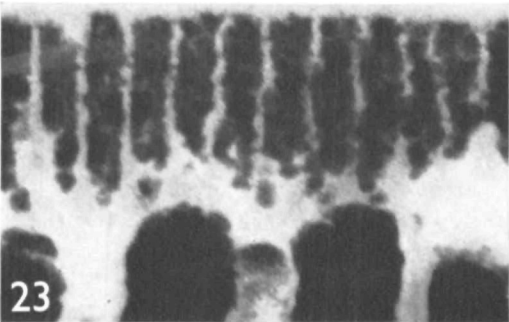
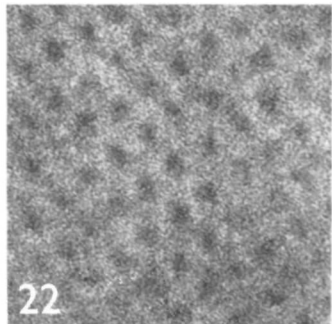
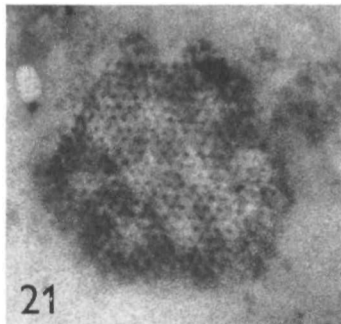
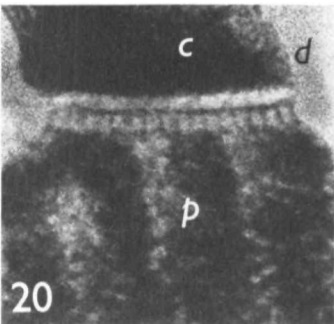
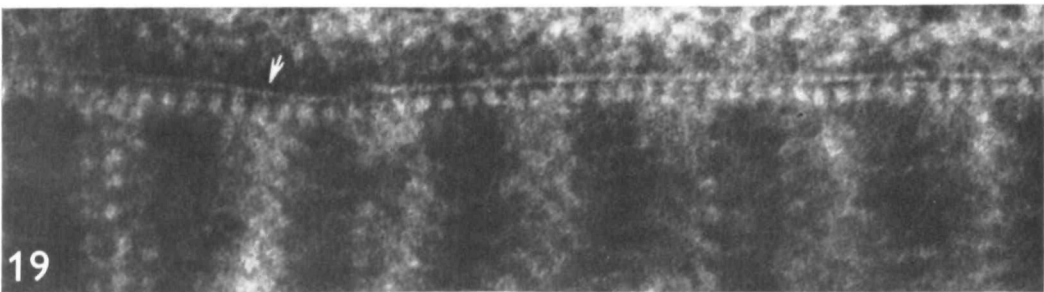
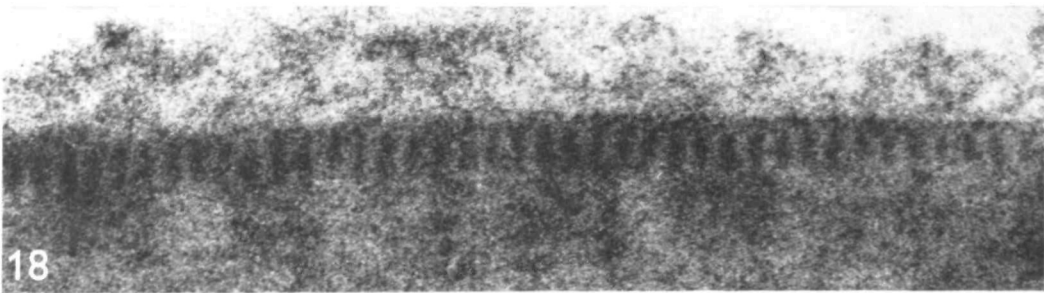
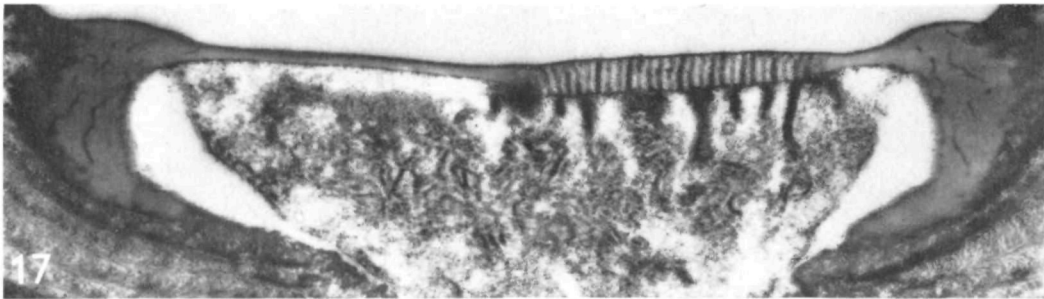
Fig. 19. The same, but infiltrated with colloidal lanthanum during fixation. The arrow points to faint striations in the light layer covering the porous lamina. $\times 400000$.

Fig. 20. Cross-section of a porous plate of *Callibaetis* after lanthanum infiltration showing a perforation site. *c*, external coat densely stained with lanthanum; *d*, dense layer material of the perforated layer; *p*, porous plate with the overlying porous lamina and light layer. $\times 300000$.

Fig. 21. The same in tangential section. Notice the tiny pores of the porous lamina and the underlying light rods of the porous plate. $\times 200000$.

Fig. 22. Porous lamina infiltrated with lanthanum in tangential section. $\times 700000$.

Figs. 23, 24. Porous plate of *Habroleptoides* fixed in the osmium-antimonate solution, showing dense precipitates within the pores and the apical cytoplasm underneath the porous plate. Fig. 23, cross-section, $\times 150000$; Fig. 24, tangential section, $\times 300000$.



- Fig. 25. Model showing the architecture of the porous plate of coniform chloride cells.
- Fig. 26. Top view photograph of the model shown in Fig. 25 (compare with Figs. 7–9, 21).
- Fig. 27. Side view photograph of the model shown in Fig. 25 (compare with Fig. 10).
- Fig. 28. Schematic representation of single and composed building units used for the construction of the model shown in Fig. 25 (see text for explanation).
- Fig. 29. Diagram of section thickness and cutting angle relative to the hexagonal pattern explaining the different patterns of the cross-sections shown in Figs. 10(a), 12(b), 13(c) and 14(d).

25

